



HAL
open science

Cyclic [Cu-biRadical] 2 Secondary Building Unit in 2p-3d and 2p-3d-4f Complexes: Crystal Structure and Magnetic Properties

Xiao-Tong Wang, Xiao-Hui Huang, Hong-Wei Song, Yue Ma, Li-Cun Li,
Jean-Pascal Sutter

► **To cite this version:**

Xiao-Tong Wang, Xiao-Hui Huang, Hong-Wei Song, Yue Ma, Li-Cun Li, et al.. Cyclic [Cu-biRadical] 2 Secondary Building Unit in 2p-3d and 2p-3d-4f Complexes: Crystal Structure and Magnetic Properties. *Molecules*, 2023, 28 (6), pp.2514. 10.3390/molecules28062514 . hal-04023710

HAL Id: hal-04023710

<https://hal.science/hal-04023710v1>

Submitted on 10 Mar 2023

HAL is a multi-disciplinary open access archive for the deposit and dissemination of scientific research documents, whether they are published or not. The documents may come from teaching and research institutions in France or abroad, or from public or private research centers.



L'archive ouverte pluridisciplinaire **HAL**, est destinée au dépôt et à la diffusion de documents scientifiques de niveau recherche, publiés ou non, émanant des établissements d'enseignement et de recherche français ou étrangers, des laboratoires publics ou privés.



Distributed under a Creative Commons Attribution 4.0 International License

Article

Cyclic [Cu-biRadical]₂ Secondary Building Unit in 2p-3d and 2p-3d-4f Complexes: Crystal Structure and Magnetic Properties

Xiao-Tong Wang¹, Xiao-Hui Huang¹, Hong-Wei Song¹, Yue Ma¹, Li-Cun Li^{1,*}  and Jean-Pascal Sutter^{2,*} 

¹ Key Laboratory of Advanced Energy Materials Chemistry, Department of Chemistry, College of Chemistry, Nankai University, Tianjin 300071, China

² Laboratoire de Chimie de Coordination du CNRS (LCC-CNRS), Université de Toulouse, Centre National de la Recherche Scientifique (CNRS), 31077 Toulouse, France

* Correspondence: llicun@nankai.edu.cn (L.-C.L.); jean-pascal.sutter@lcc-toulouse.fr (J.-P.S.)

Abstract: Employing the new nitronyl nitroxide biradical ligand biNIT-3Py-5-Ph (2-(5-phenyl-3-pyridyl)-bis(4,4,5,5-tetramethylimidazoline-1-oxyl-3-oxide)), a 16-spin Cu-radical complex, [Cu₈(biNIT-3Py-5-Ph)₄(hfac)₁₆] **1**, and three 2p-3d-4f chain complexes, {[Ln(hfac)₃][Cu(hfac)₂]₂(biNIT-3Py-5-Ph)₂]_n (Ln^{III}= Gd **2**, Tb **3**, Dy **4**; hfac = hexafluoroacetylacetonate), have been prepared and characterized. X-ray crystallographic analysis revealed in all derivatives a common cyclic [Cu-biNIT]₂ secondary building unit in which two bi-NIT-3Py-5-Ph biradical ligands and two Cu^{II} ions are associated via the pyridine N atoms and NO units. For complex **1**, two such units assemble with four additional Cu^{II} ions to form a discrete complex involving 16 S = 1/2 spin centers. For complexes **2–4**, the [Cu-biNIT]₂ units are linked by Ln^{III} ions via NO groups in a 1D coordination polymer. Magnetic studies show that the coordination of the aminoxyl groups with Cu or Ln ions results in behaviors combining ferromagnetic and antiferromagnetic interactions. No slow magnetic relaxation behavior was observed for Tb and Dy derivatives.

Keywords: nitronyl nitroxide biradical; heterospin; crystal structure; magnetic properties



Citation: Wang, X.-T.; Huang, X.-H.; Song, H.-W.; Ma, Y.; Li, L.-C.; Sutter, J.-P. Cyclic [Cu-biRadical]₂ Secondary Building Unit in 2p-3d and 2p-3d-4f Complexes: Crystal Structure and Magnetic Properties. *Molecules* **2023**, *28*, 2514. <https://doi.org/10.3390/molecules28062514>

Academic Editor: Andrzej Grzechnik

Received: 13 February 2023

Revised: 7 March 2023

Accepted: 7 March 2023

Published: 9 March 2023



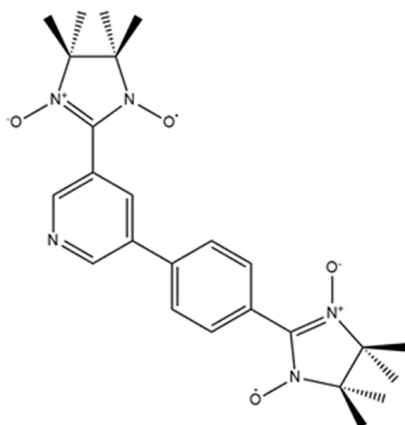
Copyright: © 2023 by the authors. Licensee MDPI, Basel, Switzerland. This article is an open access article distributed under the terms and conditions of the Creative Commons Attribution (CC BY) license (<https://creativecommons.org/licenses/by/4.0/>).

1. Introduction

A particularly promising strategy for designing molecular-exchange-coupled magnetic materials is to combine organic radicals and paramagnetic metal ions [1–3]. Utilizing this strategy, some appealing results have been achieved, among which are high-*T_C* molecular-based magnets [4,5], spin-transition-like complexes [6–10] and molecular nanomagnets, including single-molecule magnets (SMMs) and single-chain magnets (SCMs) [11–13]. Typical paramagnetic ligands are based on stable radicals such as semiquinone derivatives [14–16], nitronyl nitroxides [17–19], TCNE/TCNQ^{−1} [20–22], verdazyl radicals [23,24] and triazyls [25,26]. These radical derivatives can coordinate or even bridge paramagnetic metal ions to produce novel structures with appealing magnetic behavior, which makes them central to developments in molecular magnetism. For example, conjugated semiquinones are widely investigated in extended magnetic systems, i.e., magnets and single-molecule magnets (SMMs), due to their direct exchange mechanism based on the delocalized character of π-electrons. Slageren’s group recently reported tetraoxolene radical-bridged dinuclear Dy/Tb complexes with improved SMM behaviors due to the strong Ln–radical magnetic coupling [27]. Zheng’s group has reported the first family of *p*-semiquinone-radical-bridged lanthanide complexes, and the Dy^{III} analog exhibits a two-step slow relaxation of magnetization behavior [28]. The electron acceptor TCNQ (TCNQ = 7,7,8,8-tetracyanoquinodimethane) has been widely used as a building block by forming a stable radical in the process of designing coordination polymers and charge-transfer complexes with magnetic and electrical conducting properties [29–31]. Dunbar’s group reported TCNQ-based conductive SMMs [Dy(TPMA)(μ-TCNQ)(μ-OH)](TCNQ)₂·CH₃CN, which are the first TCNQ–rare-earth bifunctional molecular materials with high

electrical conductivity [20]. Verdazyl radicals also are employed to build molecular magnetic materials. Train et al. have obtained a six-spin cluster $[(\text{vdpy-CH}_2\text{O})_2\text{Co}_2\text{Dy}_2\text{ac}_8]$ ($\text{Hac} = \text{HO}_2\text{CCH}_3$) involving verdazyl radicals that exhibit SMM behavior [32]. It should be noted that, among all of these organic radicals, the most well-documented family of metal–radical complexes involves nitronyl nitroxide-derived ligands (NIT-R) because of the high stability and facile chemical modification of this radical. Metal complexes of 3d or 4f metal ions have been studied extensively and shown to allow a remarkable diversity of molecular architectures and appealing magnetic properties [18,33–35]. The first SCM $[\text{Co}(\text{hfac})_2(\text{NITPhOMe})]$ is constructed by using a nitronyl nitroxide radical [11]. Notably, a very large proportion of the reported nitronyl nitroxide metal complexes involve mono-radical ligands [35–42], whereas diradicals have been much less considered. However, a poly-NIT ligand possesses more coordination sites that can lead to unique assemblage topologies with metal ions and provide opportunities for the construction of novel magnetic systems. Gatteschi et al. reported a mononuclear Dy-nitronyl nitroxide biradical complex exhibiting SMM behavior [43]. A series of high-nuclear Ln-biradical SMMs were obtained by using a nitronyl nitroxide biradical involving a flexible pyridine group [44]. Wang et al. have successfully constructed Ln-based SMMs using a nitronyl nitroxide triradical [45]. More recently, 2p-4f- and 2p-3d-4f-based SCMs involving nitronyl nitroxide biradicals have been reported. Ishida and co-workers prepared a series of rare-earth chains bridged with triplet nitroxide biradicals, and a magnetic hysteresis loop was recorded for the Tb derivative [46]. Our group has also been working on the construction of SCMs using biradicals. We have shown that a biradical, with a ground spin state $S = 1$, will help to strengthen the spin-flip barrier (i.e., the activation energy for magnetization relaxation, U_{eff}) by counteracting second-neighbor interactions between two NITs coordinated to a Ln center that is antiferromagnetic in nature. Thus, a biradical-based nitronyl nitroxide-Cu–Dy chain with $U_{\text{eff}}/k_B = 40$ K could be achieved [47].

In the present paper, a new nitronyl nitroxide biradical ligand, namely, 2-(5-phenyl-3-pyridyl)-bis(4,4,5,5-tetramethylimidazoline-1-oxyl-3-oxide) (bi-NIT-3Py-5-Ph) (Scheme 1), is shown to lead to a particular cyclic dimer with Cu^{II} ions that acts as a secondary building unit (SBU) in a series of 2p-3d and 2p-3d-4f complexes. The assemblage of two such SBUs with additional Cu^{II} ions gave a discrete 16-spin complex, $[\text{Cu}_8(\text{biNIT-3Py-5-Ph})_2(\text{hfac})_{16}]$ (1), while in the presence of Ln^{III} ions, it led to the 1D coordination polymer $\{[\text{Ln}(\text{hfac})_3][\text{Cu}(\text{hfac})_2]_2(\text{biNIT-3Py-5-Ph})_2\}_n$ ($\text{Ln} = \text{Gd}$, 2; Tb, 3; Dy, 4). The preparation, crystal structures and magnetic behaviors have been investigated for all complexes.



Scheme 1. bi-NIT-3Py-5-Ph radical ligand.

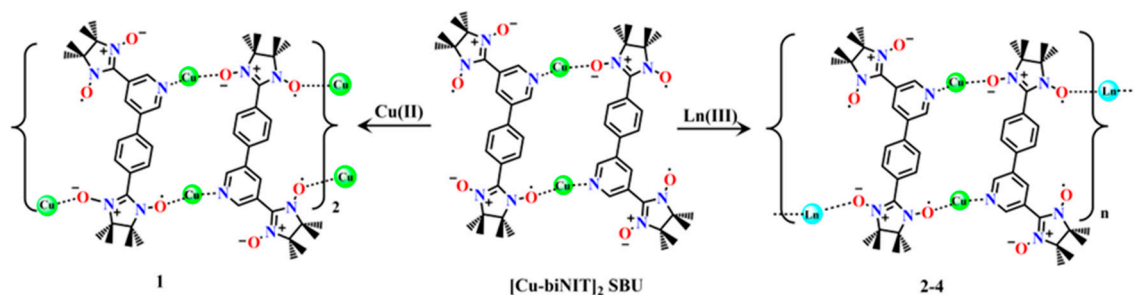
2. Results and Discussion

2.1. Spectral Properties

The IR spectra of **1–4** are shown in Figure S2. For **1**, the absorption bands of the coligand hfac[−] appear at 1252 cm^{−1} (ν_{C-F}), 1133 cm^{−1} (ν_{C-F}), 670 cm^{−1} (δ_{C-F}), 1646 cm^{−1} (ν_{C=O}) and 799 cm^{−1} (δ_{C-O}). The observed absorption peaks at 1527 cm^{−1} and 1368 cm^{−1} are assigned to C=N and N–O stretching in the biradical ligand. The IR spectra of complexes **2–4** are similar. The peaks at about 1252 cm^{−1}, 1130 cm^{−1} (ν_{C-F}), 659 cm^{−1} (δ_{C-F}), 1650 cm^{−1} (ν_{C=O}) and 798 cm^{−1} (δ_{C-O}) are assigned to the coligand hfac[−], while the peaks at about 1510 cm^{−1} and 1368 cm^{−1} originate from C=N and N–O stretching in the biradical ligand [35].

2.2. Description of the Crystal Structures

A structural feature common to all of the complexes is the occurrence of a cyclic [Cu-biNIT]₂ moiety that acts as a secondary building unit in the formation of complexes **1–4**, as depicted in Scheme 2. This unit results from the association of two biNIT-3Py-5-Ph ligands linked to two Cu^{II} ions by means of one of the NO groups and the pyridine nitrogen atom. The centrosymmetric [Cu-biNIT]₂ moiety is formed even for higher Cu^{II} stoichiometry or in the presence of other ions such as Ln^{III}, suggesting a preferred assembly pattern between biNIT-3Py-5-Ph and Cu^{II}.



Scheme 2. [Cu-biNIT]₂ SBU and its involvement in the formation of complexes **1** and **2–4**.

The single-crystal X-ray diffraction analysis reveals that complex **1** possesses a centrosymmetric structure (Figure 1) and crystallizes in the triclinic space group *P* $\bar{1}$. The asymmetric unit is composed of four Cu(hfac)₂ units and two biNIT-3Py-5-Ph ligands. The two biradical ligands are coordinated to Cu^{II} ions in different ways: one acts as a tridentate ligand in $\mu_3\text{-}\kappa\text{O}:\kappa\text{O}:\kappa\text{N}$ mode, and the other behaves as a tetradentate ligand in $\mu_4\text{-}\kappa\text{O}:\kappa\text{O}:\kappa\text{N}$ mode. Cu1 has a square-pyramidal coordination sphere, while the other three Cu^{II} ions (Cu2, Cu3 and Cu4) adopt an elongated octahedral geometry (Figure 1 and Figure S3). Cu1 is coordinated by five oxygen atoms from two hfac coligands and one NO group. One O_{hfac} atom is located in the axial site, as evidenced by the longer Cu–O_{hfac} bond (2.119(4) Å) compared to other Cu–O bond lengths (Cu–O_{rad}: 1.985(4) Å; Cu–O_{hfac}: 1.912(4)–1.970(4) Å). Both Cu2 and Cu4 have a {NO₅} coordination environment. The equatorial plane includes three O_{hfac} atoms and one N atom from pyridine (Cu–O_{hfac}: 1.939(4)–1.949(4) Å for Cu2, 1.942(4)–1.962(4) Å for Cu4, Cu–N: 2.005(4) Å for Cu2, 2.013(4) Å for Cu4). The axial positions are occupied by two oxygen atoms, one from a NO unit (Cu–O_{rad}: 2.592(4) Å for Cu2, Cu–O_{rad}: 2.489(4) Å for Cu4) and one from an hfac group (Cu–O_{hfac}: 2.217(4) Å for Cu2, Cu–O_{hfac}: 2.261(4) Å for Cu4). The Cu–O–N angles are 144.1(4)° for Cu2 and 129.2(3)° for Cu4. Cu3 is six-coordinated by four oxygen atoms from hfac groups in the equatorial plane (Cu–O_{hfac}: 1.927(4)–1.936(4) Å) and by two oxygen atoms from two NO groups in the axial positions. The latter bonds are longer (Cu–O_{rad}: 2.464(5) and 2.50(5) Å), indicating a Jahn–Teller effect [6,48]. The Cu–O–N angles are 141.2(4)° and 121.37(3)°, respectively. In the molecular complex, the shortest distance between Cu ions is 7.83(1) Å, and the separation of the uncoordinated NO group is 7.18(7) Å. The crystal packing diagram of **1** is shown in Figure S4.

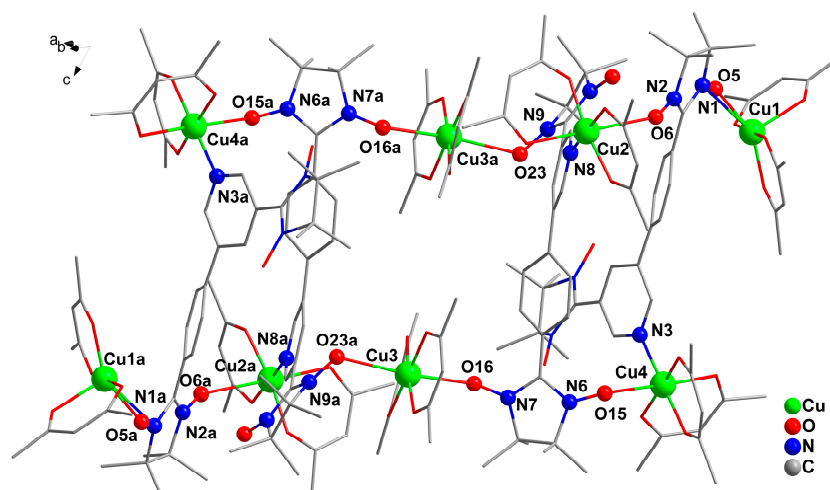


Figure 1. Crystal structure of **1** (fluorine and hydrogen atoms are omitted for the sake of clarity; symmetry code, a: x, y, 1+z).

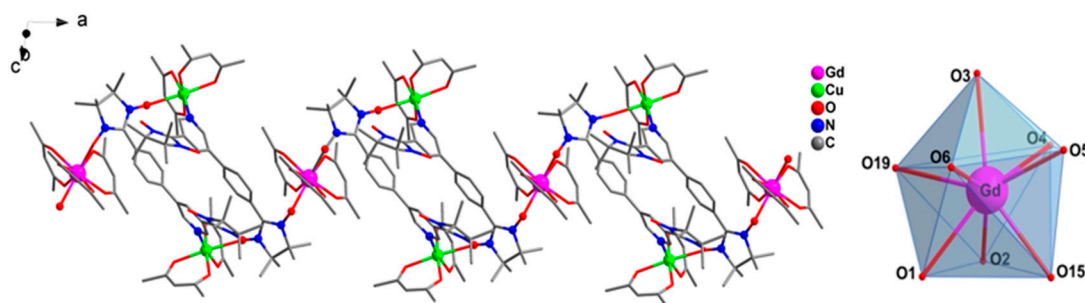


Figure 2. One-dimensional structure of **2** and coordination polyhedra of Gd^{III} ion (fluorine and hydrogen atoms are omitted for the sake of clarity).

Complexes **2–4** are isomorphous and display a one-dimensional structure (Figure 2 and Figures S5–S9). Therefore, only the structure of **2** is briefly described. Its asymmetric unit incorporates a $\text{Gd}(\text{hfac})_3$, two $\text{Cu}(\text{hfac})_2$ and two biNIT-3Py-5-Ph radical ligands. The $[\text{Cu-biNIT}]_2$ SBU formed between biNIT-3Py-5-Ph and Cu^{II} is connected to two Gd ions via the two NIT groups already linked to Cu^{II} . Likewise, each Ln center is linked to two SBUs, thus developing a zig-zag chain. Gd^{III} is eight-coordinated with two oxygen atoms from the NO groups (Gd-O_{rad} : 2.367(7) Å, 2.364(7) Å) and six oxygen atoms from three chelating hfac ligands ($\text{Gd-O}_{\text{hfac}}$: 2.358(7)–2.415(7) Å). The Gd-O-N angles are 131.9(5)° and 134.3(6)°, respectively. These distances compare well to those of the reported Ln(hfac)₃-nitronyl nitroxide complexes [40,49]. The coordination sphere around Gd has a distorted triangular dodecahedron geometry (D_{2d}), as revealed by SHAPE software [50,51] (Table 1). Each Cu^{II} ion is six-coordinated with one nitrogen, one oxygen from a NO unit and four oxygen atoms from hfac ligands. The equatorial Cu-O_{hfac} distances are between 1.930(6) and 1.975(7) Å, and the Cu-N distance is 2.003(8) Å. The axial positions are occupied by one oxygen atom from a NO group (Cu-O_{rad} : 2.519(8) Å) and another from an hfac group ($\text{Cu-O}_{\text{hfac}}$: 2.202(7) Å); these bonds are significantly longer because of the Jahn–Teller effect. In the chain, the Cu–Cu separation in the $[\text{Cu-biNIT}]_2$ unit is 9.77(2) Å, and the Gd–Cu distances are 8.52(1) Å and 8.56(2) Å. For the biradical ligand, only one of the NIT connects with metal ions. Close proximity is found between uncoordinated NO units (3.642 Å). Earlier research has indicated that the short distance of NO–NO might lead to important magnetic interactions [52,53]; however, this depends strongly on the N–O···N angle (α) and the dihedral angle (β) between the [N–O···O–N] and [O–N–C–N–O] planes [52,53]. For **2**, the angles of α and β are 112.12° and 73.96° (Figure S10) and thus incompatible with the effective overlap of magnetic orbitals, resulting in weak exchange interactions. The crystal

packing diagram of **2** is shown in Figure S5. The shortest interchain metal–metal separation is found between Cu ions with 8.00 (2) Å, and the shortest Gd–Gd and Gd–Cu distances are 16.578(9) Å and 13.84(1) Å, respectively.

Table 1. SHAPE analyses for **2–4**.

Complex	TDD-8	SAPR-8	BTPR-8	JBTPR-8
GdCu	0.369	1.572	2.040	2.607
TbCu	0.361	1.578	2.053	2.641
DyCu	0.324	1.618	2.050	2.631

2.3. Magnetic Properties

The macroscopic phase purity of each sample was confirmed by PXRD (Figure S1) before the magnetic studies. The temperature dependences of the molar magnetic susceptibilities (χ_M) were recorded between 2 and 300 K (in cooling mode) with an applied magnetic field of 1 kOe; the results are plotted as $\chi_M T$ vs. T in Figures 3–5.

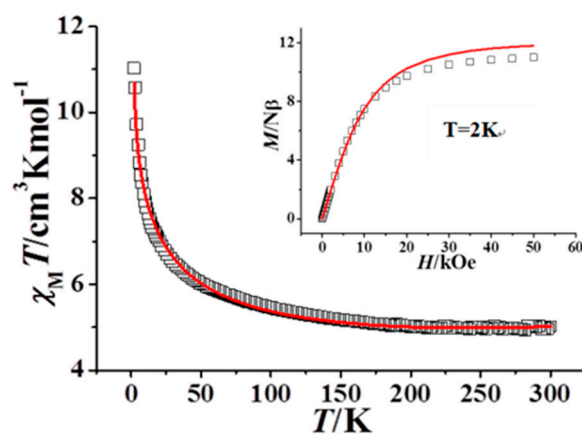


Figure 3. $\chi_M T$ vs. T and (insert) M vs. H behaviors for complex **1**. The red line is the best fit (see text).

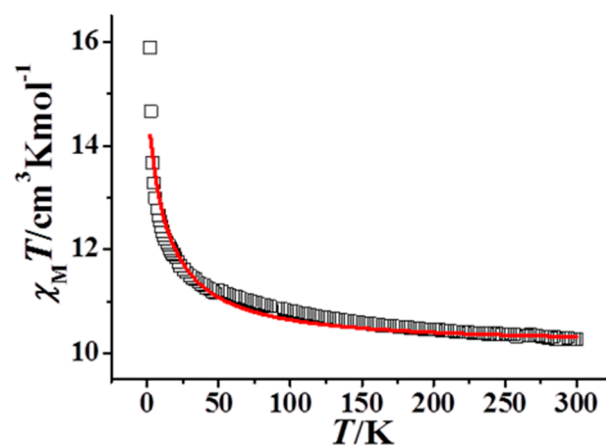


Figure 4. $\chi_M T$ vs. T plots for complex **2**. The red line is the best fit.

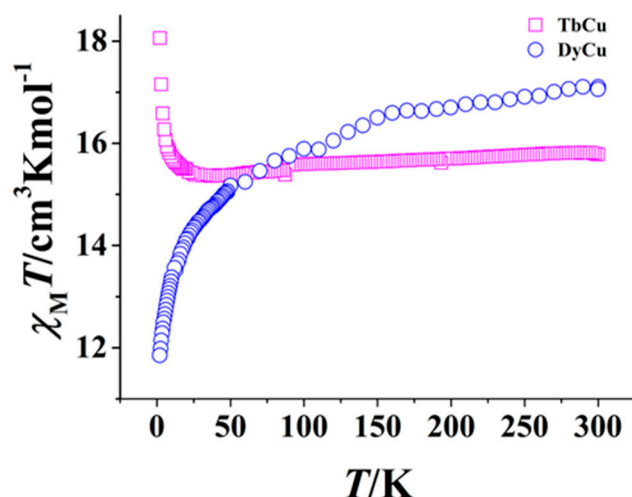
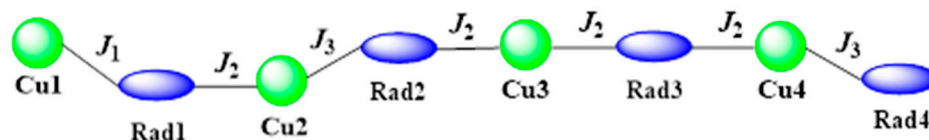


Figure 5. $\chi_M T$ vs. T plots for complexes 3 (TbCu) and 4 (DyCu).

For **1**, the overall behavior is indicative of ferromagnetic interactions within the spin system. However, the value of $\chi_M T$ obtained at 300 K ($5.01 \text{ cm}^3 \text{ K mol}^{-1}$) is clearly smaller than the expected value ($6.0 \text{ cm}^3 \text{ K mol}^{-1}$) for 16 independent $S = 1/2$ spin centers (i.e., eight Cu^{II} ions plus eight NIT radicals). This value is close to the expected contribution of $4.50 \text{ cm}^3 \text{ K mol}^{-1}$ for six free Cu^{II} ions and four monoradicals (Cu^{II} : $C = 0.375 \text{ cm}^3 \text{ K mol}^{-1}$ and $S = 1/2$; radical: $S = 1/2$). This is indicative of some strong antiferromagnetic interactions that are indeed anticipated for the equatorial Cu-NIT coordination (vide infra) in **1**. As the temperature decreases, the value of $\chi_M T$ progressively increases to reach $11.02 \text{ cm}^3 \text{ K mol}^{-1}$ at 2 K, which shows that ferromagnetic interactions are also operative in the system. The M vs. H behavior recorded at 2.0 K for fields up to 50 kOe (Figure 3) shows a very fast increase at a low field and then tends to saturate. At 50 kOe, the magnetization reaches $11.0 N\beta$, which is close to the $12 N\beta$ expected for twelve $S = 1/2$ spins, thus confirming that the contributions of four $S = 1/2$ centers have been counteracted by strong antiferromagnetic interactions.

In **1**, the magnetic exchange, if any, between the Cu^{II} ion and the NO group spaced by a pyridine and a benzene ring must be very weak, and thus, this exchange pathway can be ignored. Therefore, the magnetic behavior of this complex can be attributed to the two spin sequences comprising eight $S = 1/2$ centers in the exchange interaction, i.e., [Cu1-Rad1-Cu2-Rad2-Cu3-Rad3-Cu4-Rad4] (Scheme 3). To describe the behavior, three exchange interactions must be considered, namely, J_1 , between the Cu^{II} ions and the NO groups in the equatorial plane; J_2 , between the Cu^{II} ion and the axially coordinated NO group; and J_3 , accounting for the interaction between Cu^{II} ions and the NO group through the pyridine ring.



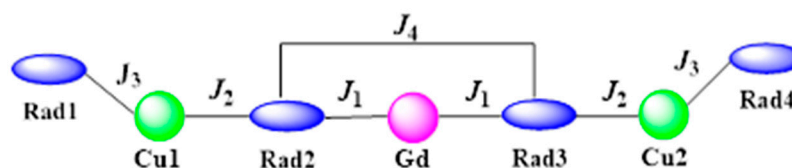
Scheme 3. Magnetic coupling pathways in complex **1**.

PHI software was employed to simultaneously analyze the $\chi_M T$ vs. T and M vs. H behaviors [54]. The best fit to the experimental data gave $J_1 = -350 (1) \text{ cm}^{-1}$, $J_2 = 25.0 (3) \text{ cm}^{-1}$, $J_3 = 2.10 (3) \text{ cm}^{-1}$, $g_{\text{Cu}} = 2.03 (1)$ and $g_{\text{rad}} = 2.0$ (fixed). The value obtained for J_1 confirms a strong and antiferromagnetic Cu- NO_{eq} interaction, which can be attributed to the effective overlap of the magnetic orbital ($d_{x^2-y^2}$) of the Cu^{II} ion and the magnetic π^* orbital of the radical [1]. The obtained value (-350 cm^{-1}) is comparable to those reported for the equatorial coordination of NIT to Cu^{II} [55–58]. The positive value for J_2 confirms

the anticipated ferromagnetic Cu-NO_{axial} interactions resulting from the orthogonality of the magnetic orbitals ($d_{x^2-y^2}$) of Cu^{II} and π^* of the radical [59]. The found strength for J_2 is consistent with the Cu-NO exchange interactions reported for similar Cu-NIT complexes [6,60,61]. The small J_3 accounts for the ferromagnetic interaction due to spin polarization between Cu^{II} and NIT through the pyridine ring [62,63].

For complexes 2–4, the $\chi_M T$ products obtained at 300 K are, respectively, 10.27 cm³ K mol⁻¹, 15.30 cm³ K mol⁻¹ and 16.87 cm³ K mol⁻¹, in good agreement with the theoretical values (10.13 cm³ K mol⁻¹ for 2, 14.07 cm³ K mol⁻¹ for 3 and 16.42 cm³ K mol⁻¹ for 4) for one Ln^{III} ion (Gd^{III}: $^8S_{7/2}$, $g = 2$, $C = 7.88$ cm³ K mol⁻¹; Tb^{III}: 7F_6 , $g = 3/2$, $C = 11.82$ cm³ K mol⁻¹; Dy^{III}: $^6H_{15/2}$, $g = 4/3$, $C = 14.17$ cm³ K mol⁻¹), two Cu^{II} ions ($S = 1/2$, $g = 2$, $C = 0.375$ cm³ K mol⁻¹) and four radicals ($S = 1/2$, $g = 2$, $C = 0.375$ cm³ K mol⁻¹) in the absence of magnetic exchange. For 2, the $\chi_M T$ value increases gradually as the temperature is lowered from 300 K to 2 K, reaching a maximum of 15.89 cm³ K mol⁻¹ (Figure 4). Such behavior is indicative of dominant ferromagnetic interactions in the system.

As mentioned above, the magnetic exchange interaction between Cu^{II} and the NIT radical through the phenyl and pyridine rings can be ignored. Thus, the magnetic properties of 2 mainly result from the exchange-coupled [Rad1-Cu1-Rad2-Gd-Rad3-Cu2-Rad4] spin sequence. The pertinent paths for magnetic interactions are shown in Scheme 4, where J_1 accounts for the Gd-NO exchange, J_2 accounts for the Cu-NO_{axial} interaction, J_3 accounts for the NO—Cu coupling via the pyridine ring, and J_4 accounts for the next-neighbor interaction between the two NO units coordinated to the Gd^{III} ion.



Scheme 4. Magnetic coupling pathways in complex 2.

The analysis of the $\chi_M T$ vs. T behavior with PHI gave $J_1 = 1.41(3)$ cm⁻¹, $J_2 = 20.3(3)$ cm⁻¹, $J_3 = 1.0(1)$ cm⁻¹, $J_4 = -6.4(1)$ cm⁻¹ and $g_{Cu} = 2.03(1)$, with $g_{rad} = g_{Gd} = 2.0$ (fixed). The positive value for J_1 indicates that the Gd-NO interaction is mainly ferromagnetic, which is attributed to a charge transfer from the π^* orbital of the radical to the empty 5d/6s orbitals of Gd, resulting in the spins of 4f and 5d (or 6s) orbitals being arranged in parallel [64–66]. The found weak ferromagnetic is in agreement with results for related Gd-NIT complexes [65,67,68]. The value obtained for J_2 confirms the ferromagnetic Cu-NO_{axial} interaction already discussed for 1, as does the positive J_3 between the Cu^{II} ion and the NO group. It is satisfying to find that 1 and 2 have very similar values for these exchange interactions. Finally, the antiferromagnetic interaction obtained for J_4 is consistent with values reported in the literature [69,70].

The M vs. H behavior was recorded at 2.0 K in a field range of 0–50 kOe (Figure S11). For 2, it is characterized by a very fast increase in magnetization for a low field and a smoother increase above 10 kOe to reach 12.4 N β at 50 kOe, close to the expected saturation value of 13 N β .

For 3, $\chi_M T$ smoothly decreases when T is reduced to 10 K and then rises rapidly to reach 18.1 cm³ K mol⁻¹ at 2 K (Figure 5). Such behavior is again indicative of ferromagnetic contributions at a low temperature, in addition to the crystal field effect applying to the Tb^{III} ion. For 4, the value of $\chi_M T$ decreases steadily from 300 to 2 K, reaching 11.85 cm³ K mol⁻¹ (Figure 5). For this derivative, the anticipated ferromagnetic Dy-ON contributions are not revealed. This overall behavior is found when the decrease due to the crystal field contribution is larger than the component of $\chi_M T$ induced by weak ferromagnetic interactions [71]. For 3 and 4, M vs. H behaviors reach values of 9.5 N β for 3 at 50 kOe and 10.8 N β for 4 at 70 kOe (Figures S12 and S13). AC magnetic susceptibility measurements for 3 and 4 performed without and with an applied static field showed no out-of-phase

(χ'') signals, thus excluding the slow relaxation of the magnetization for these derivatives (Figures S14 and S15).

3. Materials and Methods

3.1. Materials and Physical Measurements

All solvents and chemicals used in the synthesis were of analytical grade. The bi-NIT-3Py-5-Ph biradical ligand was synthesized following literature methods [72,73], and the specific synthesis process of the bi-NIT-3Py-5-Ph radical ligand is shown in Scheme S1. Elemental analysis was performed on a PerkinElmer 240 elemental analyzer. FT-IR data were obtained by using a Bruker-Vector 22 Spectrophotometer. Magnetic measurements were performed on a SQUID MPMS XL-5 and VSM magnetometer, in which samples containing Dy and Tb ions were mixed with grease to avoid orientation effects. The data were corrected for the diamagnetic contributions of the sample holder and for all of the constituent atoms using Pascal's table [74].

3.2. Synthesis of the Complexes

3.2.1. $[\text{Cu}_8(\text{biNIT-3Py-5-Ph})_4(\text{hfac})_{16}]$ (1)

$\text{Cu}(\text{hfac})_2$ (9.6 mg, 0.02 mmol) was dissolved in hot *n*-hexane (16 mL). Then, a CH_2Cl_2 solution (5.0 mL) of bi-NIT-3Py-5-Ph (3.1 mg, 0.01 mmol) was slowly added. The stirred solution was refluxed for 20 min, then cooled to room temperature and filtered. Slow evaporation of the filtrate at room temperature yielded green block-like crystals of **1**, which were isolated after 3 days (*m* = 7.8 mg, Yield: 55%). Elem. Anal. found (calcd) for $\text{C}_{180}\text{H}_{140}\text{Cu}_8\text{F}_{96}\text{N}_{20}\text{O}_{48}$ **1** (%): C 38.04, H 2.48, N 4.93; Found: C 38.21, H 2.28, N 4.39. IR (cm^{-1}): 1646 (s), 1527 (m), 1458 (s), 1368 (m), 1252 (s), 1199 (s), 1133 (s), 799 (s), 670 (s), 590 (s), 528 (m).

3.2.2. $\{[\text{Gd}(\text{hfac})_3][\text{Cu}(\text{hfac})_2]_2(\text{biNIT-3Py-5-Ph})_2\}_n$ (2)

A solution of $\text{Gd}(\text{hfac})_3 \cdot 2\text{H}_2\text{O}$ (8.2 mg, 0.01 mmol) and $\text{Cu}(\text{hfac})_2$ (9.6 mg, 0.02 mmol) in heptane (18 mL) was heated to reflux for 3 h. Then, a CHCl_3 solution (10 mL) of bi-NIT-3Py-5-Ph (6.2 mg, 0.02 mmol) was slowly added. The resulting solution was further refluxed for 15 min, then cooled to room temperature and filtered. The filtrate evaporated slowly at room temperature over a period of 4 days to give gray-purple strip crystals of the chain complex. For **2**: *m* = 14.7 mg, Yield = 55%. Elem. Anal. found (calcd) (%) for $\text{C}_{85}\text{H}_{69}\text{Cu}_2\text{F}_{42}\text{GdN}_{10}\text{O}_{22}$: C 38.31, H 2.61, N 5.26; Found: C 38.04, H 2.10, N 5.48. IR (cm^{-1}): 1650 (s), 1510 (m), 1368 (m), 1253 (s), 1200 (s), 1138 (s), 912 (m), 869 (m), 798 (s), 659 (s), 585 (s), 545 (m).

3.2.3. $\{[\text{Tb}(\text{hfac})_3][\text{Cu}(\text{hfac})_2]_2(\text{biNIT-3Py-5-Ph})_2\}_n$ (3)

Samples of $\text{Tb}(\text{hfac})_3 \cdot 2\text{H}_2\text{O}$ (8.2 mg, 0.01 mmol) and $\text{Cu}(\text{hfac})_2$ (9.6 mg, 0.02 mmol) were dissolved in boiling *n*-heptane (20 mL) and heated to reflux for 4 h. Then, a CHCl_3 solution (10 mL) of bi-NIT-3Py-5-Ph (6.2 mg, 0.02 mmol) was added. The obtained solution was refluxed for 12 min. The solution was filtered, allowed to cool down and evaporated at room temperature for 4 days. Gray-purple strip crystals of the chain complexes were obtained. For **3**: *m* = 15.47 mg, Yield = 58%. Elem. Anal. found (calcd) (%) for $\text{C}_{85}\text{H}_{69}\text{Cu}_2\text{F}_{42}\text{TbN}_{10}\text{O}_{22}$: C 38.29, H 2.61, N 5.25; Found: C 38.13, H 2.36, N 5.42. IR (cm^{-1}): 1650 (s), 1508 (m), 1368 (m), 1250 (s), 1200 (s), 1137 (s), 913 (m), 870 (m), 798 (s), 659 (s), 585 (s), 545 (m).

3.2.4. $\{[\text{Dy}(\text{hfac})_3][\text{Cu}(\text{hfac})_2]_2(\text{biNIT-3Py-5-Ph})_2\}_n$ (4)

$\text{Dy}(\text{hfac})_3 \cdot 2\text{H}_2\text{O}$ (8.2 mg, 0.01 mmol) and $\text{Cu}(\text{hfac})_2$ (9.6 mg, 0.02 mmol) dissolved in hot *n*-heptane (20 mL) for refluxing were added to a CHCl_3 solution (12 mL) of bi-NIT-3Py-5-Ph (6.2 mg, 0.02 mmol) with further reflux for 20 min. The solution was filtered and allowed to stay at room temperature for 3 days. Well-shaped gray-purple strip crystals suitable for X-ray structure determination were obtained. For **4**: *m* = 14.42 mg, Yield = 54%.

Elem. Anal. found (calcd) (%) for $C_{85}H_{69}Cu_2F_{42}DyN_{10}O_{22}$: C 38.24, H 2.60, N 5.24; Found: C 38.05, H 2.30, N 5.56. IR (cm^{-1}): 1650 (s), 1509 (m), 1370 (m), 1250 (s), 1200 (s), 1130 (s), 906 (m), 870 (m), 798 (s), 659 (s), 582 (s), 528 (m).

3.3. X-Ray Structure Determination

Single-crystal X-ray data of complexes 1–4 were collected at 113 K on a Rigaku Saturn CCD diffractometer with graphite monochromated Mo-K α radiation ($\lambda = 0.71073 \text{ \AA}$). The single-crystal structure was solved by SHELXL-2014 [75] and SHELXS 2014 [76] programs. All non-hydrogen atoms were refined anisotropically, and the H atoms of organic molecules were positioned geometrically. SIMU, DELU, ISOR and other commands were used to correct some disordered C and F atoms. Crystallographic data for complexes 1–4 are shown in Table 2. Key bond lengths and angles are listed in Table 3, Table 4 and Tables S1–S4, respectively.

Table 2. Crystallographic data for complexes 1–4.

Complex	1	2	3	4
Formula	$C_{90}H_{70}Cu_4F_{48}N_{10}O_{24}$	$C_{85}H_{69}Cu_2F_{42}GdN_{10}O_{22}$	$C_{81}H_{53}Cu_2F_{42}TbN_{10}O_{22}O_{22}$	$C_{81}H_{53}Cu_2F_{42}DyN_{10}O_{22}$
$Mr, g \cdot mol^{-1}$	2841.72	2664.83	2666.50	2670.08
T/K	113(2)	113(2)	113(2)	113(2)
Crystal system	Triclinic	Monoclinic	Monoclinic	Monoclinic
Space group	$P\bar{1}$	$P2_1/n$	$P2_1/n$	$P2_1/n$
$a/\text{\AA}$	16.9339(5)	15.2072(4)	15.1947(4)	15.2346(4)
$b/\text{\AA}$	18.6148(7)	26.5688(7)	26.6157(4)	26.6466(6)
$c/\text{\AA}$	20.4094(8)	30.2985(9)	30.2844(7)	30.2582(7)
$\alpha/^\circ$	71.591(3)	90	90	90
$\beta/^\circ$	71.330(3)	99.343(3)	99.0810(17)	98.792(2)
$\gamma/^\circ$	89.533(3)	90	90	90
$V/\text{\AA}^3$	5752.0(4)	12,079.3(6)	12,094.0(5)	12,139.0(5)
Z	2	4	4	4
$D_{calcd}/g \cdot cm^{-3}$	1.641	1.465	1.465	1.461
$\mu(mm^{-1})$	0.878	1.018	1.054	1.083
$\theta/^\circ$	1.648–26.372	1.559–24.713	1.531–24.713	1.611–24.713
$F(000)$	2840	5300	5304	5308
Reflections collected	61,762	47,646	91,466	84,653
Unique reflns/Rint	23,530/0.0599	19,859/0.0556	20,584/0.0692	20,681/0.1009
GOF (F^2)	0.98	1.001	1.002	1.021
$R_1/wR_2 [I > 2\sigma(I)]^a$	0.0702/0.1518	0.1024/0.2331	0.0760/0.1975	0.0795/0.1964
R_1/wR_2 (All data) ^a	0.1288/0.1935	0.1310/0.2449	0.0929/0.2060	0.1187/0.2223

$$^a R_1 = \sum(|F_o| - |F_c|) / \sum|F_o|. wR_2 = [\sum w(|F_o|^2 - |F_c|^2)^2 / \sum w|F_o|^2]^2$$

Table 3. Key bond lengths [\AA] and angles [$^\circ$] for complex 1.

Complex	1 Cu
Cu1-O _{rad} , Cu2-O _{rad}	1.985(4), 2.592(4)
Cu3-O _{rad}	2.464(5), 2.506(5)
Cu4-O _{rad}	2.489(4)
Cu2-N, Cu4-N	2.005(4), 2.013(4)
Cu1-O _{hfac}	1.912(4)–2.119(4)
Cu2-O _{hfac}	1.939(4)–2.217(4)
Cu3-O _{hfac}	1.927(4)–1.936(4)
Cu4-O _{hfac}	1.942(4)–2.261(4)
N-O _{rad} -Cu1, N-O _{rad} -Cu2	119.8(3), 144.1(4)
N-O _{rad} -Cu3	141.2(4), 121.4(3)
N-O _{rad} -Cu4	129.2(5)
N-Cu2-O _{rad} , N-Cu4-O _{rad}	88.70(16), 90.19(15)
O _{rad} -Cu2-N, O _{rad} -Cu4-N	88.72(2), 90.19(2)
O _{rad} -Cu3-O _{rad}	163.7(2)

Table 4. Key bond lengths [Å] and angles [°] for complexes 2–4.

Complex	2 GdCu	3 TbCu	4 DyCu
Ln-O _{rad}	2.367(7), 2.364(7)	2.369(5), 2.355(5)	2.358(5), 2.337(5)
Ln-O _{hfac}	2.358(7)–2.415(7)	2.366(5)–2.398(5)	2.347(5)–2.392(5)
Ln-O-N	131.9(5), 134.3(6)	132.6(4), 134.9(4)	133.1(5), 134.3(5)
O _{rad} -Ln-O _{rad}	141.0(2)	141.05(16)	140.92(19)
Cu-O _{rad}	1.930(6)–2.202(7)	1.944(5)–2.201(5)	1.942(5)–2.206(6)
Cu-O _{hfac}	1.940(7)–2.249(8)	1.945(5)–2.253(6)	1.937(6)–2.259(8)
Cu-N	2.003(8), 2.034(8)	2.012(5), 2.020(6)	2.019(6), 2.034(7)
Cu-O _{rad}	2.519(8), 2.509(8)	2.506(6), 2.493(6)	2.522(6), 2.493(7)
Cu-O-N	157.4(7), 153.3(7)	157.5(5), 154.6(5)	157.5(5), 156.5(5)
N-Cu-O	87.7(3), 88.1(3)	87.3(2), 87.6(2)	87.6(2), 86.5(2)

4. Conclusions

The reported diradical ligand was found to interact with Cu^{II} ions to form a specific cyclic [CubiNIT]₂ dimer, and this unit then acts as an SBU in the formation of polynuclear complexes. A 16-spin Cu-NIT complex and a series of 2p-Cu-Ln 1D complexes were derived from this particular association pattern induced by the biNIT-3Py-5-Ph ligand. In the 2p-3d complex, the biNIT-3Py-5-Ph diradical ligands behave as three- or four-dentate ligands to bind Cu^{II} ions, leading to an octanuclear structure. In the 2p-3d-4f complexes, the cyclic [Cu-radical]₂ dimers connect Ln ions via NO groups to develop a 1D coordination polymer. Magnetic studies have shown that there exist strong antiferromagnetic and ferromagnetic interactions stemming from the Cu-NO_{eq} and Cu-NO_{axial} moieties, respectively, in complex 1. For 2–3, the magnetic behaviors are governed by ferromagnetic NO-Ln/Cu interactions. This work demonstrates that nitronyl nitroxide diradicals containing functional groups are appealing ligands for constructing novel radical–metal complexes with interesting spin topologies.

Supplementary Materials: The following supporting information can be downloaded at: <https://www.mdpi.com/article/10.3390/molecules28062514/s1>. CCDC deposition numbers: CCDC 2224151–2224154 contain the supplementary crystallographic data for 1–4, respectively. These data can be obtained free of charge from The Cambridge Crystallographic Data Centre via www.ccdc.cam.ac.uk/data_request/cif (accessed on 6 February 2023). Tables S1–S4: Selected bond lengths [Å] and angles [°] for 1–4; Figure S1: The Powder X-ray diffraction (PXRD) patterns for all complexes at room temperature; Figure S2: The IR spectra for complexes 1–4. Figure S3: The coordination polyhedra of Cu^{II} ions; Figures S4–S9: The Packing diagrams and the one-dimensional structures of complexes 1–4; Figure S10: The relative disposition and the close contacts between the uncoordinated NO groups in 2. Figures S11–S13: Field-dependent magnetization for complexes 2–4. Figures S14–S15: Frequency-dependent ac signals of the χ' (top) and χ'' (bottom) for complexes 3–4; Scheme S1: The synthesis of bi-NIT-3Py-5-Ph radical ligand.

Author Contributions: Investigation: X.-T.W., X.-H.H., H.-W.S. and Y.M.; data collection and analysis: J.-P.S., X.-H.H. and X.-T.W.; writing—review and editing: X.-T.W., L.-C.L. and J.-P.S.; funding acquisition: L.-C.L. All authors have read and agreed to the published version of the manuscript.

Funding: This work was financially supported by the National Natural Science Foundation of China (No. 21773122).

Institutional Review Board Statement: Not applicable.

Informed Consent Statement: Not applicable.

Data Availability Statement: Data is contained within the article or supplementary material.

Conflicts of Interest: The authors declare no conflict of interest.

Sample Availability: Samples of the compounds 1–4 are available from the authors.

References

1. Caneschi, A.; Gatteschi, D.; Sessoli, R.; Rey, P. Toward molecular magnets: The metal-radical approach. *Acc. Chem. Res.* **1989**, *22*, 392–398. [[CrossRef](#)]
2. Demir, S.; Jeon, I.-R.; Long, J.R.; Harris, T.D. Radical ligand-containing single-molecule magnets. *Coord. Chem. Rev.* **2015**, *289–290*, 149–176. [[CrossRef](#)]
3. Thorarinsdottir, A.E.; Harris, T.D. Metal–Organic Framework Magnets. *Chem. Rev.* **2020**, *120*, 8716–8789. [[CrossRef](#)]
4. Inoue, K.; Hayamizu, T.; Iwamura, H.; Hashizume, D.; Ohashi, Y. Assemblage and Alignment of the Spins of the Organic Trinitroxide Radical with a Quartet Ground State by Means of Complexation with Magnetic Metal Ions. A Molecule-Based Magnet with Three-Dimensional Structure and High T_C of 46 K. *J. Am. Chem. Soc.* **1996**, *118*, 1803–1804. [[CrossRef](#)]
5. Fegy, K.; Luneau, D.; Ohm, T.; Paulsen, C.; Rey, P. Two-Dimensional Nitroxide-Based Molecular Magnetic Materials. *Angew. Chem. Int. Ed.* **1998**, *37*, 1270–1273. [[CrossRef](#)]
6. Lanfranc de Panthou, F.; Belorizky, E.; Calemczuk, R.; Luneau, D.; Marcenat, C.; Ressouche, E.; Turek, P.; Rey, P. A New Type of Thermally Induced Spin Transition Associated with an Equatorial. d_{blarw}. Axial Conversion in a Copper(II)-Nitroxide Cluster. *J. Am. Chem. Soc.* **1995**, *117*, 11247–11253. [[CrossRef](#)]
7. Lanfranc de Panthou, F.; Luneau, D.; Musin, R.; Öhrström, L.; Grand, A.; Turek, P.; Rey, P. Spin-Transition and Ferromagnetic Interactions in Copper(II) Complexes of a 3-Pyridyl-Substituted Imino Nitroxide. Dependence of the Magnetic Properties upon Crystal Packing. *Inorg. Chem.* **1996**, *35*, 3484–3491. [[CrossRef](#)]
8. Kaszub, W.; Marino, A.; Lorenc, M.; Collet, E.; Bagryanskaya, E.G.; Tretyakov, E.V.; Ovcharenko, V.I.; Fedin, M.V. Ultrafast Photoswitching in a Copper-Nitroxide-Based Molecular Magnet. *Angew. Chem. Int. Ed.* **2014**, *53*, 10636–10640. [[CrossRef](#)]
9. Fedin, M.V.; Veber, S.L.; Maryunina, K.Y.; Romanenko, G.V.; Suturina, E.A.; Gritsan, N.P.; Sagdeev, R.Z.; Ovcharenko, V.I.; Bagryanskaya, E.G. Intercluster Exchange Pathways in Polymer-Chain Molecular Magnets Cu(hfac)₂L-R Unveiled by Electron Paramagnetic Resonance. *J. Am. Chem. Soc.* **2010**, *132*, 13386–13891. [[CrossRef](#)]
10. Zhu, M.; Li, C.; Wang, X.; Li, L.; Sutter, J.-P. Thermal Magnetic Hysteresis in a Copper–Gadolinium–Radical Chain Compound. *Inorg. Chem.* **2016**, *55*, 2676–2678. [[CrossRef](#)]
11. Caneschi, A.; Gatteschi, D.; Lalioti, N.; Sangregorio, C.; Sessoli, R.; Venturi, G.; Vindigni, A.; Rettori, A.; Pini, M.G.; Novak, M.A. Cobalt(II)-nitronyl nitroxide chains as molecular magnetic nanowires. *Angew. Chem. Int. Ed.* **2001**, *40*, 1760–1763. [[CrossRef](#)]
12. Patrascu, A.A.; Briganti, M.; Soriano, S.; Calancea, S.; Allão Cassaro, R.A.; Totti, F.; Vaz, M.G.F.; Andruh, M. SMM Behavior Tuned by an Exchange Coupling LEGO Approach for Chimeric Compounds: First 2p–3d–4f Heterotriscipin Complexes with Different Metal Ions Bridged by One Aminoxyl Group. *Inorg. Chem.* **2019**, *58*, 13090–13101. [[CrossRef](#)]
13. Kanegawa, S.; Karasawa, S.; Maeyama, M.; Nakano, M.; Koga, N. Crystal Design of Monometallic Single-Molecule Magnets Consisting of Cobalt-Aminoxyl Heterospins. *J. Am. Chem. Soc.* **2008**, *130*, 3079–3094. [[CrossRef](#)] [[PubMed](#)]
14. Bencini, A.; Caneschi, A.; Dei, A.; Gatteschi, D.; Sangregorio, C.; Shultz, D.; Sorace, L.; Vaz, M.G.F. Polyoxolenes may provide a tool for designing paramagnetic molecules with predetermined spin topologies. *Comptes Rendus Chim.* **2003**, *6*, 663–676. [[CrossRef](#)]
15. Dei, A.; Gatteschi, D.; Sangregorio, C.; Sorace, L. Quinonoid Metal Complexes: Toward Molecular Switches. *Acc. Chem. Res.* **2004**, *37*, 827–835. [[CrossRef](#)]
16. Ovcharenko, V.I.; Gorelik, E.V.; Fokin, S.V.; Romanenko, G.V.; Ikorskii, V.N.; Krashilina, A.V.; Cherkasov, V.K.; Abakumov, G.A. Ligand Effects on the Ferro- to Antiferromagnetic Exchange Ratio in Bis(o-Semiquinonato) copper(II). *J. Am. Chem. Soc.* **2007**, *129*, 10512–10521. [[CrossRef](#)]
17. Iwamura, H.; Koga, N. Studies of organic di-, oligo-, and polyradicals by means of their bulk magnetic properties. *Acc. Chem. Res.* **1993**, *26*, 346–351. [[CrossRef](#)]
18. Luneau, D.; Rey, P. Magnetism of metal-nitroxide compounds involving bis-chelating imidazole and benzimidazole substituted nitronyl nitroxide free radicals. *Coord. Chem. Rev.* **2005**, *249*, 2591–2611. [[CrossRef](#)]
19. Baskett, M.; Paduan-Filho, A.; Oliveira, N.F., Jr.; Chandrasekaran, A.; Mague, J.T.; Lahti, P.M. Loops, Chains, Sheets, and Networks from Variable Coordination of Cu(hfac)₂ with a Flexibly Hinged Aminoxyl Radical Ligand. *Inorg. Chem.* **2011**, *50*, 5060–5074. [[CrossRef](#)] [[PubMed](#)]
20. Zhang, X.; Wang, Z.-X.; Xie, H.-M.; Li, M.-X.; Woods, T.J.; Dunbar, K.R. A cobalt(ii) spin-crossover compound with partially charged TCNQ radicals and an anomalous conducting behavior. *Chem. Sci.* **2016**, *7*, 1569–1574. [[CrossRef](#)]
21. Pokhodnya, K.I.; Bonner, M.; Her, J.H.; Stephens, P.W.; Miller, J.S. Magnetic ordering ($T_c = 90$ K) observed for layered [Fe^{II}(TCNE^{•-})(NCMe)₂]⁺[Fe^{III}Cl₄]⁻ (TCNE = Tetracyanoethylene). *J. Am. Chem. Soc.* **2006**, *128*, 15592–15593. [[CrossRef](#)]
22. Miller, J.S. Zero-dimensional organic-based magnets possessing decamethylmetallocene. *J. Mater. Chem.* **2010**, *20*, 1846–1857. [[CrossRef](#)]
23. Wang, C.; Lin, S.-Y.; Shi, W.; Cheng, P.; Tang, J.-K. Exploiting verdazyl radicals to assemble 2p–3d–4f one-dimensional chains. *Dalton Trans.* **2015**, *44*, 5364–5368. [[CrossRef](#)]
24. Brook, D.J.R.; Lynch, V.; Conklin, B.; Fox, M.A. Spin Delocalization in the Copper(I) Complexes of Bis(verdazyl) Diradicals. *J. Am. Chem. Soc.* **1997**, *119*, 5155–5162. [[CrossRef](#)]
25. Fujita, W.; Awaga, K. Ferromagnetic Coordination Polymer Composed of Heterocyclic Thiazyl Radical, 1,3,5-Trithia-2,4,6-triazapentalenyl (TTA), and Bis(hexafluoroacetylacetonato) copper(II) (Cu(hfac)₂). *J. Am. Chem. Soc.* **2001**, *123*, 3601–3602. [[CrossRef](#)] [[PubMed](#)]

26. Alberola, A.; Less, R.J.; Pask, C.M.; Rawson, J.M.; Palacio, F.; Oliete, P.; Paulsen, C.; Yamaguchi, A.; Farley, R.D.; Murphy, D.M. A Thiazyl-Based Organic Ferromagnet. *Angew. Chem. Int. Ed.* **2003**, *42*, 4782–4785. [[CrossRef](#)] [[PubMed](#)]
27. Zhang, P.; Perfetti, M.; Kern, M.; Hallmen, P.P.; Ungur, L.; Lenz, S.; Ringenberg, M.R.; Frey, W.; Stoll, H.; Rauhut, G.; et al. Exchange coupling and single molecule magnetism in redox-active tetraoxolene-bridged dilanthanide complexes. *Chem. Sci.* **2018**, *9*, 1221–1230. [[CrossRef](#)] [[PubMed](#)]
28. Han, T.; Wang, X.-Q.; Chai, Y.-C.; Zheng, Y.-Z. Slow Relaxation of Magnetization in a p-Semiquinone Radical-Bridged Dysprosium Complex. *Cryst. Growth Des.* **2023**, *23*, 24–30. [[CrossRef](#)]
29. Zhang, X.; Xie, H.; Ballesteros-Rivas, M.; Woods, T.J.; Dunbar, K.R. Conducting Molecular Nanomagnet of Dy^{III} with Partially Charged TCNQ Radicals. *Chem. Eur. J.* **2017**, *23*, 7448–7452. [[CrossRef](#)]
30. Üngör, Ö.; Burrows, M.; Liu, T.; Bodensteiner, M.; Adhikari, Y.; Hua, Z.; Casas, B.; Balicas, L.; Xiong, P.; Shatruk, M. Paramagnetic Molecular Semiconductors Combining Anisotropic Magnetic Ions with TCNQ Radical Anions. *Inorg. Chem.* **2021**, *60*, 10502–10512. [[CrossRef](#)] [[PubMed](#)]
31. Zhang, X.; Saber, M.R.; Prosvirin, A.P.; Reibenspies, J.H.; Sun, L.; Ballesteros-Rivas, M.; Zhao, H.; Dunbar, K.R. Magnetic ordering in TCNQ-based metal–organic frameworks with host–guest interactions. *Inorg. Chem. Front.* **2015**, *2*, 904–911. [[CrossRef](#)]
32. Novitchi, G.; Shova, S.; Lan, Y.; Wernsdorfer, W.; Train, C. Verdazyl Radical, a Building Block for a Six-Spin-Center 2p–3d–4f Single-Molecule Magnet. *Inorg. Chem.* **2016**, *55*, 12122–12125. [[CrossRef](#)] [[PubMed](#)]
33. Vostrikova, K.E.; Luneau, D.; Wernsdorfer, W.; Rey, P.; Verdaguer, M. A S = 7 Ground Spin-State Cluster Built from Three Shells of Different Spin Carriers Ferromagnetically Coupled, Transition-Metal Ions and Nitroxide Free Radicals. *J. Am. Chem. Soc.* **2000**, *122*, 718–719. [[CrossRef](#)]
34. Bogani, L.; Sangregorio, C.; Sessoli, R.; Gatteschi, D. Molecular Engineering for Single-Chain-Magnet Behavior in a One-Dimensional Dysprosium–Nitronyl Nitroxide Compound. *Angew. Chem. Int. Ed.* **2005**, *44*, 5817–5821. [[CrossRef](#)]
35. Bernot, K.; Bogani, L.; Caneschi, A.; Gatteschi, D.; Sessoli, R. A Family of Rare-Earth-Based Single Chain Magnets: Playing with Anisotropy. *J. Am. Chem. Soc.* **2006**, *128*, 7947–7956. [[CrossRef](#)]
36. Zhou, N.; Ma, Y.; Wang, C.; Xu, G.F.; Tang, J.-K.; Xu, J.-X.; Yan, S.-P.; Cheng, P.; Li, L.-C.; Liao, D.-Z. A monometallic tri-spin single-molecule magnet based on rare earth radicals. *Dalton Trans.* **2009**, *40*, 8489–8492. [[CrossRef](#)] [[PubMed](#)]
37. Coronado, E.; Giménez-Saiz, C.; Recuenco, A.; Tarazón, A.; Romero, F.M.; Camón, A.; Luis, F. Single-Molecule Magnetic Behavior in a Neutral Terbium(III) Complex of a Picolinate-Based Nitronyl Nitroxide Free Radical. *Inorg. Chem.* **2011**, *50*, 7370–7372. [[CrossRef](#)]
38. Wang, X.-L.; Li, L.-C.; Liao, D.-Z. Slow Magnetic Relaxation in Lanthanide Complexes with Chelating Nitronyl Nitroxide Radical. *Inorg. Chem.* **2010**, *49*, 4735–4737. [[CrossRef](#)] [[PubMed](#)]
39. Murakami, R.; Ishida, T.; Yoshii, S.; Nojiri, H. Single-molecule magnet [Tb(hfac)₃(2pyNO)] (2pyNO = t-butyl 2-pyridyl nitroxide) with a relatively high barrier of magnetization reversal. *Dalton Trans.* **2013**, *42*, 13968–13973. [[CrossRef](#)]
40. Poneti, G.; Bernot, K.; Bogani, L.; Caneschi, A.; Sessoli, R.; Wernsdorfer, W.; Gatteschi, D. A rational approach to the modulation of the dynamics of the magnetisation in a dysprosium–nitronyl-nitroxide radical complex. *Chem. Commun.* **2007**, *18*, 1807–1809. [[CrossRef](#)]
41. Pointillart, F.; Bernot, K.; Poneti, G.; Sessoli, R. Crystal Packing Effects on the Magnetic Slow Relaxation of Tb(III)-Nitronyl Nitroxide Radical Cyclic Dinuclear Clusters. *Inorg. Chem.* **2012**, *51*, 12218–12229. [[CrossRef](#)] [[PubMed](#)]
42. Xi, L.; Han, J.; Huang, X.-H.; Li, L.-C. Nitronyl Nitroxide Biradical-Based Binuclear Lanthanide Complexes: Structure and Magnetic Properties. *Magnetochemistry* **2020**, *6*, 48. [[CrossRef](#)]
43. Bernot, K.; Pointillart, F.; Rosa, P.; Etienne, M.; Sessoli, R.; Gatteschi, D. Single molecule magnet behaviour in robust dysprosium-biradical complexes. *Chem. Commun.* **2010**, *46*, 6458–6460. [[CrossRef](#)] [[PubMed](#)]
44. Xi, L.; Li, H.; Sun, J.; Ma, Y.; Tang, J.-K.; Li, L.-C. Designing Multicoordinating Nitronyl Nitroxide Radical Toward Multinuclear Lanthanide Aggregates. *Inorg. Chem.* **2020**, *59*, 443–451. [[CrossRef](#)]
45. Xiao, Z.-X.; Miao, H.; Shao, D.; Wei, H.-Y.; Zhang, Y.-Q.; Wang, X.-Y. Single-molecule magnet behaviour in a dysprosium-triradical complex. *Chem. Commun.* **2018**, *54*, 9726–9729. [[CrossRef](#)]
46. Ito, S.; Takano, R.; Hatanaka, S.-i.; Ishida, T. Rare-Earth (RE = Y, Gd, Tb, Dy, Ho, and Er) Chains Bridged with a Triplet Biradical and Magnetic Hysteresis Recorded for RE = Tb. *Inorg. Chem.* **2022**, *61*, 10619–10623. [[CrossRef](#)] [[PubMed](#)]
47. Xie, J.; Li, H.-D.; Yang, M.; Sun, J.; Li, L.-C.; Sutter, J.-P. Improved single-chain-magnet behavior in a biradical-based nitronyl nitroxide-Cu–Dy chain. *Chem. Commun.* **2019**, *55*, 3398–3401. [[CrossRef](#)]
48. Wang, H.-M.; Liu, Z.-L.; Liu, C.-M.; Zhang, D.-Q.; Lü, Z.-L.; Geng, H.; Shuai, Z.-G.; Zhu, D.-B. Coordination Complexes of 2-(4-Quinolyl) nitronyl Nitroxide with M(hfac)₂ [M = Mn(II), Co(II), and Cu(II)]: Syntheses, Crystal Structures, and Magnetic Characterization. *Inorg. Chem.* **2004**, *43*, 4091–4098. [[CrossRef](#)] [[PubMed](#)]
49. Yang, M.; Sun, J.; Guo, J.-N.; Sun, G.-F.; Li, L.-C. Cu–Ln compounds based on nitronyl nitroxide radicals: Synthesis, structure, and magnetic and fluorescence properties. *CrystEngComm* **2016**, *18*, 9345–9356. [[CrossRef](#)]
50. Llunell, M.; Casanova, D.; Circa, J.; Bofill, J.; Alcmay, P.; Alvarez, S.; Pinsky, M.; Avnir, D. *SHAPE*, version 2.1; University of Barcelona: Barcelona, Spain; Hebrew University of Jerusalem: Jerusalem, Israel, 2005.
51. Casanova, D.; Llunell, M.; Alemany, P.; Alvarez, S. The Rich Stereochemistry of Eight-Vertex Polyhedra: A Continuous Shape Measures Study. *Chem. Eur. J.* **2005**, *11*, 1479–1494. [[CrossRef](#)]

52. Caneschi, A.; Ferraro, F.; Gatteschi, D.; Rey, P.; Sessoli, R. Crystal structure and magnetic properties of a copper(II) chloride nitronyl nitroxide complex containing six exchange-coupled $S = 1/2$ spins. *Inorg. Chem.* **1990**, *29*, 1756–1760. [[CrossRef](#)]
53. Fettouhi, M.; El Ali, B.; El-Ghanam, A.M.; Golhen, S.; Ouahab, L.; Daro, N.; Sutter, J.-P. Temperature Dependence of the Crystal Lattice Organization of Coordination Compounds Involving Nitronyl Nitroxide Radicals: A Magnetic and Structural Investigation. *Inorg. Chem.* **2002**, *41*, 3705–3712. [[CrossRef](#)] [[PubMed](#)]
54. Chilton, N.F.; Anderson, R.P.; Turner, L.D.; Soncini, A.; Murray, K.S. PHI: A powerful new program for the analysis of anisotropic monomeric and exchange-coupled polynuclear d- and f-block complexes. *J. Comput. Chem.* **2013**, *34*, 1164–1175. [[CrossRef](#)] [[PubMed](#)]
55. Caneschi, A.; Gatteschi, D.; Hoffman, S.K.; Laugier, J.; Rey, P.; Sessoli, R. Crystal and molecular structure, magnetic properties and EPR spectra of a trinuclear copper(II) complex with bridging nitronyl nitroxides. *Inorg. Chem.* **1988**, *27*, 2390–2392. [[CrossRef](#)]
56. Fokin, S.; Ovcharenko, V.; Romanenko, G.; Ikorskii, V. Problem of a Wide Variety of Products in the $\text{Cu}(\text{hfac})_2$ –Nitroxide System. *Inorg. Chem.* **2004**, *43*, 969–977. [[CrossRef](#)]
57. Zhang, Y.-J.; Wang, J.-J.; Huang, Q.; Chen, J. Crystal structures and magnetic properties of nitronyl nitroxide NiT_2 -phtrz and its M(II) hexafluoroacetylacetonate (M = manganese, copper) complexes $[\text{M}(\text{hfac})_2(\text{NiT}_2\text{-phtrz})]$. *Transit. Met. Chem.* **2012**, *37*, 743–749. [[CrossRef](#)]
58. Li, H.-D.; Lu, J.; Xie, J.; Jing, P.; Li, L.-C. Two-Dimensional Nitronyl Nitroxide–Cu Networks Based on Multi-Dentate Nitronyl Nitroxides: Structures and Magnetic Properties. *Magnetochemistry* **2021**, *7*, 73. [[CrossRef](#)]
59. Luneau, D.; Rey, P.; Laugier, J.; Fries, P.; Caneschi, A.; Gatteschi, D.; Sessoli, R. Nitrogen-bonded copper(II)-imino nitroxide complexes exhibiting large ferromagnetic interactions. *J. Am. Chem. Soc.* **1991**, *113*, 1245–1251. [[CrossRef](#)]
60. Caneschi, A.; Ferraro, F.; Gatteschi, D.; Rey, P.; Sessoli, R. Structure and Magnetic Properties of a Chain Compound Formed by Copper (II) and a Tridentate Nitronyl Nitroxide Radical. *Inorg. Chem.* **1991**, *30*, 3162–3166. [[CrossRef](#)]
61. Sun, J.; Xi, L.; Xie, J.; Wang, K.; Li, L.C.; Sutter, J.P. A loop chain and a three-dimensional network assembled from a multi-dentate nitronyl nitroxide radical and $\text{M}(\text{hfac})_2$ (M = Co-II, Cu-II). *Dalton Trans.* **2018**, *47*, 14630–14635. [[CrossRef](#)]
62. Souza, D.A.; Moreno, Y.; Ponzio, E.A.; Resende, J.A.L.C.; Jordão, A.K.; Cunha, A.C.; Ferreira, V.F.; Novak, M.A.; Vaz, M.G.F. Synthesis, crystal structure, magnetism and electrochemical properties of two copper(II) furoyltrifluoroacetate complexes with nitroxide radical. *Inorg. Chim. Acta* **2011**, *370*, 469–473. [[CrossRef](#)]
63. Xu, Y.-H.; Qu, X.-N.; Song, H.-B.; Li, L.-C.; Jiang, Z.-H.; Liao, D.-Z. Metal–radical complexes $[\text{M}(\text{NiTm-Py})_2(\text{N}_3)_2(\text{DMSO})_2]$ [M=Cu(II), Ni(II), Co(II)]: Syntheses, crystal structures and magnetic properties. *Polyhedron* **2007**, *26*, 741–747. [[CrossRef](#)]
64. Gupta, T.; Rajeshkumar, T.; Rajaraman, G. Magnetic exchange in $\{\text{Gd}^{\text{III}}\text{-radical}\}$ complexes: Method assessment, mechanism of coupling and magneto-structural correlations. *Phys. Chem. Chem. Phys.* **2014**, *16*, 14568–14577. [[CrossRef](#)]
65. Benelli, C.; Caneschi, A.; Gatteschi, D.; Pardi, L.; Rey, P.; Shum, D.P.; Carlin, R.L. Magnetic properties of lanthanide complexes with nitronyl nitroxides. *Inorg. Chem.* **1989**, *28*, 272–275. [[CrossRef](#)]
66. Andruh, M.; Ramade, I.; Codjovi, E.; Guillou, O.; Kahn, O.; Trombe, J.C. Crystal structure and magnetic properties of $[\text{Ln}_2\text{Cu}_4]$ hexanuclear clusters (where Ln = trivalent lanthanide). Mechanism of the gadolinium(III)-copper(II) magnetic interaction. *J. Am. Chem. Soc.* **1993**, *115*, 1822–1829. [[CrossRef](#)]
67. Benelli, C.; Caneschi, A.; Gatteschi, D.; Pardi, L. Gadolinium(III) complexes with pyridine-substituted nitronyl nitroxide radicals. *Inorg. Chem.* **1992**, *31*, 741–746. [[CrossRef](#)]
68. Lu, J.; Jing, P.; Jin, C.; Xie, J.; Li, L. Modulating the magnetization dynamics in Ln–Cu–Rad hetero-tri-spin complexes through cis/trans coordination of nitronyl nitroxide radicals around the metal center. *Dalton Trans.* **2021**, *50*, 3280–3288. [[CrossRef](#)] [[PubMed](#)]
69. Benelli, C.; Caneschi, A.; Gatteschi, D.; Pardi, L.; Rey, P. Linear-chain gadolinium(III) nitronyl nitroxide complexes with dominant next-nearest-neighbor magnetic interactions. *Inorg. Chem.* **1990**, *29*, 4223–4228. [[CrossRef](#)]
70. Sutter, J.P.; Kahn, M.L.; Golhen, S.; Ouahab, L.; Kahn, O. Synthesis and Magnetic Behavior of Rare-Earth Complexes with N,O-Chelating Nitronyl Nitroxide Triazole Ligands: Example of a $[\text{Gd}^{\text{III}}\{\text{Organic Radical}\}_2]$ Compound with an $S=9/2$ Ground State. *Chem. Eur. J.* **1998**, *4*, 571–576. [[CrossRef](#)]
71. Sutter, J.P.; Kahn, M.L.; Kahn, O. Conclusive Demonstration of the Ferromagnetic Nature of the Interaction Between Holmium(III) and Aminoxyl Radicals. *Adv. Mater.* **1999**, *11*, 863–865. [[CrossRef](#)]
72. Davis, M.S.; Morokuma, K.; Kreilick, R.W. Free radicals with large negative spin densities. *J. Am. Chem. Soc.* **1972**, *94*, 5588–5592. [[CrossRef](#)]
73. Meier, P.; Legraverant, S.; Muller, S.; Schaub, J. Synthesis of formylphenylpyridinecarboxylic acids using Suzuki-Miyaura coupling reactions. *Synthesis* **2003**, *4*, 551–554. [[CrossRef](#)]
74. Kahn, O. *Molecular Magnetism*; VCH: Weinheim, Germany, 1993.
75. Sheldrick, G.M. *SHELXS-2014, Program for Structure Solution*; Universität of Göttingen: Göttingen, Germany, 2014.
76. Sheldrick, G.M. *SHELXL-2014, Program for Structure Refinement*; Universität of Göttingen: Göttingen, Germany, 2014.

Disclaimer/Publisher’s Note: The statements, opinions and data contained in all publications are solely those of the individual author(s) and contributor(s) and not of MDPI and/or the editor(s). MDPI and/or the editor(s) disclaim responsibility for any injury to people or property resulting from any ideas, methods, instructions or products referred to in the content.